Automatika

Journal for Control, Measurement, Electronics, Computing and Communications

ISSN: 0005-1144 (Print) 1848-3380 (Online) Journal homepage: https://www.tandfonline.com/loi/taut20

Hopf bifurcation, antimonotonicity and amplitude controls in the chaotic Toda jerk oscillator: analysis, circuit realization and combination synchronization in its fractional-order form

Justin Roger Mboupda Pone, Sifeu Takougang Kingni, Guy Richard Kol & Viet-Thanh Pham

To cite this article: Justin Roger Mboupda Pone, Sifeu Takougang Kingni, Guy Richard Kol & Viet-Thanh Pham (2019) Hopf bifurcation, antimonotonicity and amplitude controls in the chaotic Toda jerk oscillator: analysis, circuit realization and combination synchronization in its fractional-order form, Automatika, 60:2, 149-161, DOI: 10.1080/00051144.2019.1600109

To link to this article: https://doi.org/10.1080/00051144.2019.1600109

Published online: 15 Apr 2019.

AUTOMATIKA
2019, VOL. 60, NO. 2, 149–161
https://doi.org/10.1080/00051144.2019.1600109

Taylor & Francis
Taylor & Francis Group

REGULAR PAPER

OPEN ACCESS Check for updates

Hopf bifurcation, antimonotonicity and amplitude controls in the chaotic Toda jerk oscillator: analysis, circuit realization and combination synchronization in its fractional-order form

Justin Roger Mboupda Pone[a], Sifeu Takougang Kingni[b], Guy Richard Kol[b,c] and Viet-Thanh Pham[d]

[a]Research Unit of Automation and Applied Computer, Electrical Engineering Department of IUT-FV of Bandjoun, University of Dschang, Dschang, Cameroon; [b]Department of Mechanical, Petroleum and Gas Engineering, Faculty of Mines and Petroleum Industries, University of Maroua, Maroua, Cameroon; [c]School of Geology and Mining Engineering, University of Ngaoundere, Ngaoundere, Cameroon; [d]Nonlinear Systems and Applications, Faculty of Electrical & Electronics Engineering, Ton Duc Thang University, Ho Chi Minh City, Vietnam

ABSTRACT

In this paper, an autonomous Toda jerk oscillator is proposed and analysed. The autonomous Toda jerk oscillator is obtained by converting an autonomous two-dimensional Toda oscillator with an exponential nonlinear term to a jerk oscillator. The existence of Hopf bifurcation is established during the stability analysis of the unique equilibrium point. For a suitable choice of the parameters, the proposed autonomous Toda jerk oscillator can generate antimonotonicity, periodic oscillations, chaotic oscillations and bubbles. By introducing two additional parameters in the proposed autonomous Toda jerk oscillator, it is possible to control partially or totally the amplitude of its signals. In addition, electronic circuit realization of the proposed Toda jerk oscillator is carried out to confirm results found during numerical simulations. The commensurate fractional-order version of the proposed autonomous chaotic Toda jerk oscillator is studied using the stability theorem of fractional-order oscillators and numerical simulations. It is found that periodic oscillations and chaos exist in the fractional-order form of the proposed Toda jerk oscillator with order less than three. Finally, combination synchronization of two fractional-order proposed autonomous chaotic Toda jerk oscillators with another fractional-order proposed autonomous chaotic Toda jerk oscillator is analysed using the nonlinear feedback control method.

ARTICLE HISTORY
Received 13 November 2018
Accepted 18 March 2019

KEYWORDS
Chaotic jerk oscillator; Hopf bifurcation; antimonotonicity; partial or total amplitude control; fractional-order form; combination synchronization

1. Introduction

Chaotic oscillations can be generated in the third-order or higher-order autonomous nonlinear differential equations. In the case of non-autonomous differential equations, i.e. nonlinear damped systems driven by external periodic voltage, the minimal order of the differential equations can be reduced to two. Chaos was found useful with great potential in many fields, including liquid mixing with low power consumption, human brain and heartbeat regulation, and secure communications [1–5]. In electrical circuits, chaotic oscillations have been observed and intensively investigated, but the circuits considered lead to difficult electronic implementations. Since 2000, the development of new autonomous chaotic oscillators with easy electronic implementation has been of interest, as it is shown in Sprott's paper [6]. Sprott [7] proposed many new jerk systems with several nonlinearities that show chaotic behaviour with easy electronic implementation. In one of the chapter of "Elegant Chaos: Algebraically Simple flow", book published in 2010, Sprott proposed a list of 16 autonomous jerk oscillators with different nonlinearities called memory oscillators (MO_0 to MO_{15}) [8]. He gave the value of parameters for which these MOs can exhibit chaos and plotted the phase portraits of the chaotic attractors of each oscillator. These nonlinearities of MOs are quadratic, cubic, quintic, absolute, maximum, sign, exponential, sine hyperbolic and tangent hyperbolic functions. However, the results of [8] are restricted on the presentation of the rate-equations of chaotic memory oscillators and make no mention on the chaotic mechanism of each MO. The authors of [9,10] introduced, theoretically studied and experimented two autonomous chaotic oscillators using the Van der Pol dynamics immersed into a jerk oscillator. These two jerk oscillators belong to the family of MO_5. This MO is a chaotic jerk oscillator with cubic nonlinearity. In [11,12], authors proposed, theoretically studied and experimented an autonomous chaotic Duffing oscillator based on a jerk system which belongs to the family of MO_5. Kengne et al. proposed, numerically analysed and experimented a chaotic jerk oscillator

CONTACT Justin Roger Mboupda Pone mboupdapone00@gmail.com Research Unit of Automation and Applied Computer, Electrical Engineering Department of IUT-FV of Bandjoun, University of Dschang, P.O. Box 134 Bandjoun, Dschang, Cameroon

with hyperbolic sine nonlinearity which belongs to the family of MO_{15} in [13].

Motivated by the above works, in this paper, an autonomous chaotic jerk oscillator is obtained by converting an autonomous two-dimensional Toda oscillator into a three-dimensional differential equations using the jerk architecture which belongs to the family of MO_{11}. This memory oscillator is a simple autonomous jerk oscillator with exponential nonlinearity. The Toda oscillator is a two-dimensional differential equation describing an oscillator with exponential nonlinearity. The Toda equation is a model of CO_2 and solid state lasers [14–16]. In the classical Toda oscillator with external periodic signal, the period-doubling route to chaos has been observed [17]. However, the frequency generator used to provide the external periodic signal is not always easy to obtain because it is expensive. The proposed autonomous jerk oscillator can provide wide benefits compared to the classical Toda oscillator with external periodic signal in some applications where the space to put all the devices can be very small as a system on a chip for example. On the dynamical point of view, a chaotic behaviour generated by an oscillator driven by a periodic signal is not indicated for some relevant engineering applications such as secure communications because of the presence of the driven frequency in the secure signal. The power spectrum of chaos found in an autonomous oscillator has a randomly distributed harmonics peaks indicating the robustness of the chaotic signal [8,18,19]. To the best of author's knowledge, there is not work in the literature on theoretical and experimental analysis of integer and fractional autonomous jerk oscillator with exponential nonlinearity. Therefore, in this paper, the integer and fractional autonomous Toda jerk oscillator is analysed in order to understand the dynamics of this class of jerk oscillator with exponential nonlinearity. Our objective in this work is divided twofold. Firstly, give more light on the dynamics of the proposed autonomous Toda jerk oscillator with experimental verifications. Secondly, dynamical behaviour and combination synchronization in its fractional-order form investigation using the stability theory of fractional-order oscillators [20] and numerical simulations based on the Adams–Bashforth–Moulton predictor corrector scheme [21–23].

The paper is organized as follows. Section 2 is devoted to the analytical and numerical analysis of the autonomous Toda jerk oscillator under investigation. In Section 3, an electronic circuit is designed and realized for the investigation of the dynamical behaviour of the autonomous Toda Jerk oscillator. Section 4 focuses on analysis of the effect of fractional derivation on the chaos found in the proposed Toda jerk oscillator and the combination synchronization of the proposed Toda jerk oscillator with two other proposed Toda jerk oscillators. The conclusion is given in section 5.

2. Description and analysis of the autonomous Toda jerk oscillator

Motivated by the simplicity of the jerk systems and that it is easy to build its corresponding analogue computer, we proposed and analysed in this section a three-dimensional oscillator based on the jerk architecture derive from the Toda two-dimensional oscillator. A Jerk oscillator is a three-dimensional differential equation of the form [6,23–30]:

$$\dddot{x} = f(\ddot{x}, \dot{x}, x), \tag{1}$$

where x, $\dot{x}$, $\ddot{x}$ and $\dddot{x}$ represent the dynamical variables, first-, second-, third-order time derivative, respectively. The autonomous two-dimensional Toda oscillator is given by [19]

$$\ddot{x} + \alpha\dot{x} - 1 + \exp(x) = 0, \tag{2}$$

which is a two-dimensional differential equation. The parameter α is a dimensionless damping coefficient ($\alpha > 0$). It is well known in the literature that for any value of parameter α, the trajectories of Equation (2) converge asymptotically to its only equilibrium point $(x(0) = 0, y(0) = \dot{x}(0) = 0)$.

$$\dddot{x} = -[\ddot{x} + \alpha\dot{x} - 1 + \exp(x)]. \tag{3}$$

The Toda equation can be converted to a jerk oscillator using the famous method to transform the two-dimensional non-autonomous oscillator into an autonomous oscillator. The state space representation of the novel jerk oscillator yields:

$$\dot{x} = y, \tag{4a}$$

$$\dot{y} = \beta z, \tag{4b}$$

$$\dot{z} = -z - \alpha y + 1 - \exp(x), \tag{4c}$$

where $\dot{x}(t) = y(t)$ and $\ddot{x}(t) = z(t)$. The positive constant parameter β is added in order to generate chaotic behaviour in system (4).

2.1. Analytical study

System (4) is dissipative because $\nabla V = \partial\dot{x}/\partial x + \partial\dot{y}/\partial y + \partial\dot{z}/\partial z = -1 < 0$. It has only one equilibrium point $O = (0, 0, 0)$. The characteristic equation derived from the Jacobian matrix at O is

$$\lambda^3 + \lambda^2 + \alpha\beta\lambda + \beta = 0. \tag{5}$$

Using the Routh–Hurwitz criteria, this equation has all roots with negative real parts if and only if:

$$\beta > 0, \tag{6a}$$

$$(\alpha - 1)\beta > 0. \tag{6b}$$

Since $\alpha > 0$, the equilibrium point $O = (0, 0, 0)$ of system (4) is stable if $\alpha > 1$ and unstable for $\alpha < 1$. In

the following paragraph, we study the Hopf bifurcation from equilibrium point O regarding α as the bifurcation parameter.

Theorem: *If $\beta > 0$, system (4) has a Hopf bifurcation at equilibrium point O when α passes through the critical value $\alpha_H = 1$.*

Proof: Replacing $\lambda = \mathrm{j}\omega$ ($\omega > 0$ and $\mathrm{j}^2 = -1$) into Equation (5) and separating real and imaginary parts, we obtain ■

$$\omega = \omega_0 = \sqrt{\beta}, \tag{7a}$$

$$\alpha_H = 1. \tag{7b}$$

Differentiating both sides of Equation (5) with respect to α gives

$$3\lambda^2 \frac{\mathrm{d}\lambda}{\mathrm{d}\alpha} + 2\lambda \frac{\mathrm{d}\lambda}{\mathrm{d}\alpha} + \alpha\beta \frac{\mathrm{d}\lambda}{\mathrm{d}\alpha} + \beta\lambda = 0 \tag{8a}$$

and

$$\frac{\mathrm{d}\lambda}{\mathrm{d}\alpha} = \frac{-\beta\lambda}{3\lambda^2 + 2\lambda + \alpha\beta}, \tag{8b}$$

then

$$\mathrm{Re}\left(\left. \frac{\mathrm{d}\lambda}{\mathrm{d}\alpha} \right|_{\alpha=\alpha_H,\, \lambda=\mathrm{i}\omega_0} \right) = -\frac{1}{4} \neq 0. \tag{8c}$$

Since the Jacobian matrix of system (4) at the equilibrium point O has two purely imaginary eigenvalues and the real parts of eigenvalues satisfy Re $(\mathrm{d}\lambda/\mathrm{d}\alpha|_{\alpha=\alpha_H,\, \lambda=\mathrm{i}\omega_0}) \neq 0$; all the conditions for Hopf bifurcation to occur are satisfied. Consequently, system (4) has a Hopf bifurcation at O when $\alpha = \alpha_H = 1$ and periodic solutions will exist in a neighbourhood of the point α_H (provided that $\beta > 0$ holds). For $\alpha = 1.05 > \alpha_H$, the trajectories of system (4) converge to the equilibrium point O, whereas for $\alpha = 0.9 < \alpha_H$, system (4) exhibits a limit cycle (not shown).

2.2. Numerical study

The dynamical behaviours of system (4) can be illustrated by numerical bifurcation diagrams, Lyapunov exponents, phase portraits and first-return map. We choose parameters α and β as the control parameters. We fix $\beta = 5$ and vary parameter α. In Figure 1, we present the bifurcation diagram depicting local extrema of $x(t)$ and the largest Lyapunov exponent versus parameter α.

When the parameter α varies from 0.165 to 1.1, the bifurcation diagram of the output $x(t)$ in Figure 1(a) displays period-1-oscillations followed by period-doubling to chaos interspersed with periodic windows. By further increasing the parameter α, system (4) undergoes a reverse period-doubling bifurcation and a period-1-oscillation is observed up to $\alpha \approx 1$, where a Hopf bifurcation occurs followed by converging of the trajectories of system (4) to the equilibrium point $O = (0, 0, 0)$. The chaotic behaviour is confirmed by the largest Lyapunov exponent shown in Figure 1(b). We plot in Figure 2, the phase portraits of chaotic oscillations for specific values of α and β.

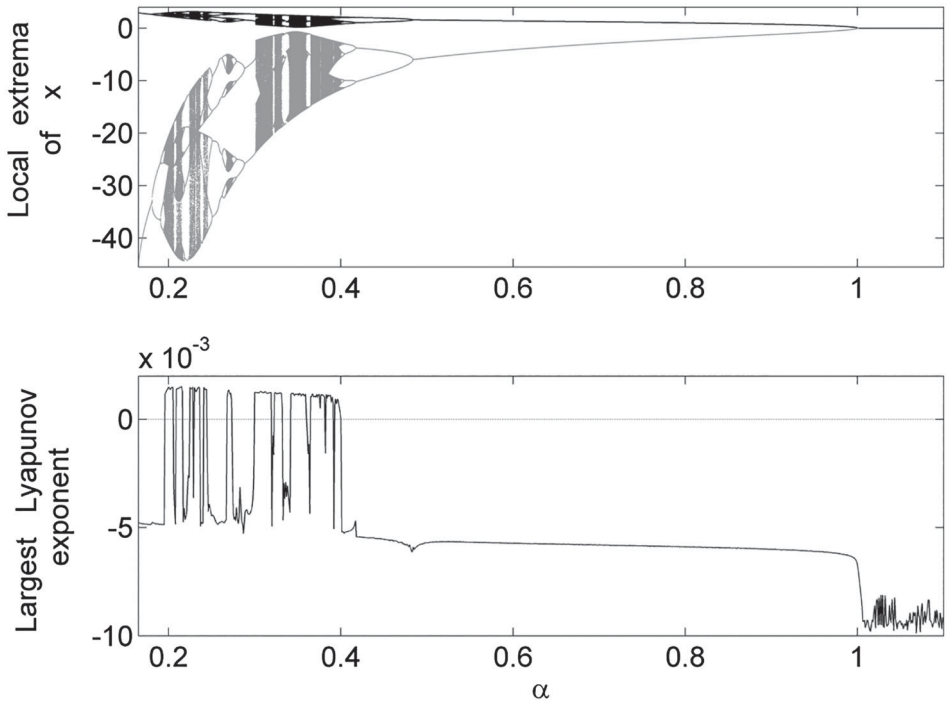

Figure 1. Bifurcation diagram depicting the local maxima (black dots) and local minima (grey dots) of $x(t)$ (a) and the largest Lyapunov exponent (b) versus parameter α for $\beta = 5$.

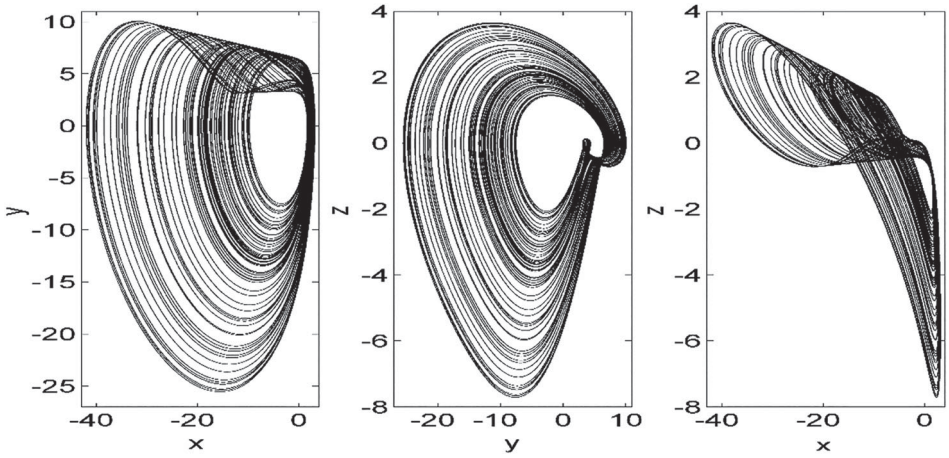

Figure 2. Phase portraits of system (4) in planes (x, y), (y, z) and (x, z) with $\beta = 5$ and $\alpha = 0.235$. Initial conditions $(x(0), y(0), z(0)) = (0.1, 0.1, 0.1)$.

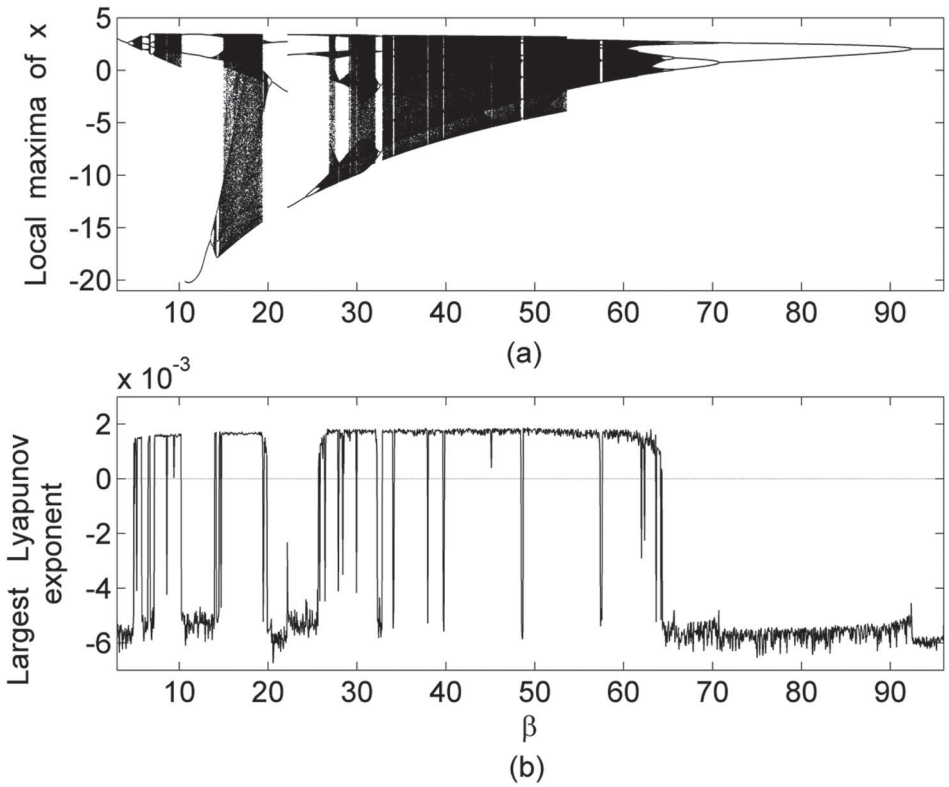

Figure 3. Bifurcation diagram depicting the local maxima of $x(t)$ (a) and the largest Lyapunov exponent (b) versus the parameter β for $\alpha = 0.2$.

From Figure 2, one can notice that the trajectories of the chaotic attractor of system (4) are swirling around equilibrium point O. This is a signature of one-scroll chaotic attractor. For $\alpha = 0.2$, we plot as shown in Figure 3 the bifurcation diagram of $x(t)$ and the largest Lyapunov exponent versus the newly introduced parameter β.

When the parameter β increases from 3 to 96 [see Figure 3(a)], the bifurcation diagram of the output $x(t)$ shows period-1-oscillation followed by period-doubling bifurcation to chaos for $4.86 < \beta < 19.52$. The chaotic region is interspersed with five main periodic windows. Then a reverse period-doubling bifurcation is observed followed by period-2-oscillations from $\beta \approx 20.38$ until $\beta \approx 24.8105$ where a chaotic behaviour occurs. For parameter $\beta > 24.8105$, period-6-oscillations is watched followed by period-doubling bifurcation to chaos interspersed with periodic windows. By further increasing parameter β, system (4) undergoes a reverse period-doubling bifurcation and a period-1-oscillation are observed for $\beta > 92.41$. These forward and reverse period-doubling sequences, as a parameter of system (4) increases in a monotone way, are called antimonotonicity [31–34].

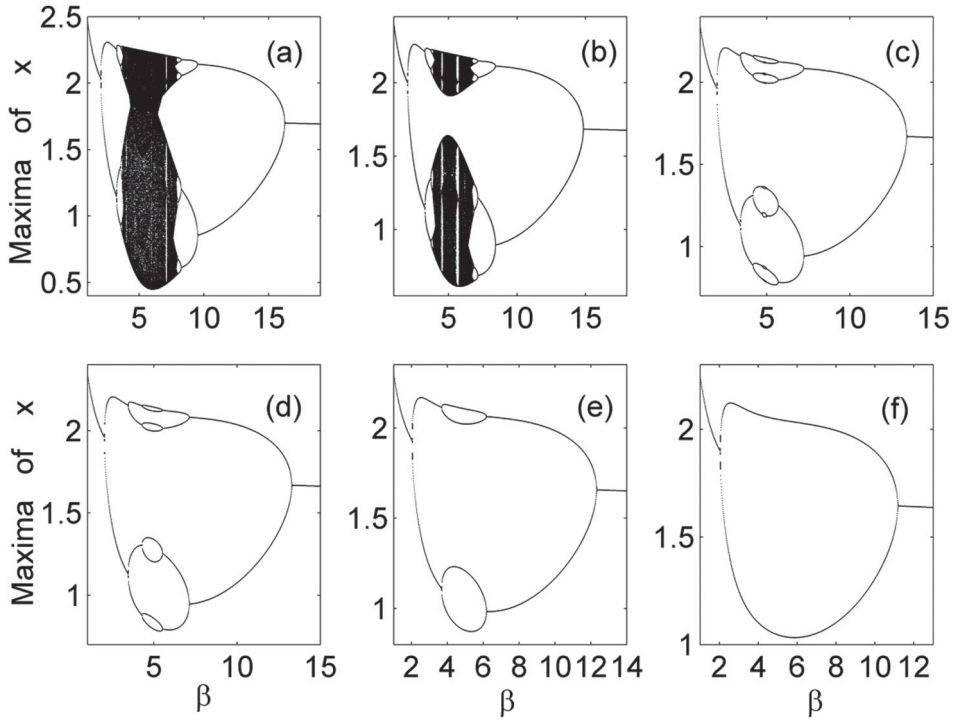

Figure 4. Bifurcation diagrams depicting the local maxima of $x(t)$ versus parameter β for specific values of parameter α: (a) unique chaotic oscillations at $\alpha = 0.38$, (b) two chaotic bubbles at $\alpha = 0.39$, (c) bubble of period 16 at $\alpha = 0.401$, (d) bubble of period 8 at $\alpha = 0.402$, (e) bubble of period 4 at $\alpha = 0.41$ and (f) bubble of period 2 at $\alpha = 0.42$.

The chaotic behaviour is confirmed by the largest Lyapunov exponent shown in Figure 3(b).

2.3. Antimonotonicity phenomenon

The term antimonotonicity has been coined by Dawson et al. [33] to characterize creation and annihilation of periodic orbits, via reverse bifurcation sequences as a parameter is increased in nonlinear dynamical systems. Dawson et al. [34] have proposed a geometric mechanism called dimple formations a possible means for antimonotonicity in one-dimensional maps that contain two critical points inside the chaotic attractor. Thus, in order to demonstrate the existence of the antimonotonicity phenomenon in the proposed autonomous Toda Jerk oscillator, the bifurcation diagrams depicting the maxima of $x(t)$ versus parameter β are computed for some specific values of parameter α as depicted in Figure 4.

In the bifurcation diagrams of Figure 4(a) and (b) chaotic oscillations and chaotic bubbles [31] are depicted respectively, while in the bifurcation diagrams of Figure 4(c)–(f), only periodic states (periodic bubbles) are found. For $\alpha = 0.42$, system (4) undergoes the sequence: period-1-oscillation $\rightarrow$ period-2-oscillations $\rightarrow$ period-1-oscillation. Bier and Bountis [31] named this sequence as "primary bubble". The chaotic bubble shown in Figure 4(b) is further detailed in Figure 5, which depicts the phase portrait of the resulting chaotic attractor of system (4) in plane (x, y), (y, z), (x, z) and the first-return map of the local maxima of $x(t)$ for specific values of parameters α and β.

The chaotic bubbles attractor is presented in Figure 5(a)–(c) where one can note that the trajectories of the chaotic attractor of system (4) are swirling around equilibrium point O and the shape of the attractors of Figure 5 are different to the one of chaotic attractors of Figure 2. The chaotic behaviour is confirmed by the numerical calculation of the Lyapunov exponents which gives $LE_1 \approx 0.0527, LE_2 \approx 0$ and $LE_3 \approx -1.0527$. The Lyapunov dimension of the chaotic bubbles is $D_{KY} \approx 2.0500$. In Figure 5(d), the map is indicative of one-dimensional maps with two critical points p_1 and p_2, which support the occurrence of the antimonotonicity phenomenon in the proposed autonomous Toda Jerk oscillator according to the results of Dawson et al. [34].

2.4. Partial and total amplitude control

Oscillators with partial and total amplitude controls are of great interest for some engineering applications where the desired amplitude level can be achieved by using one or two constant parameters. This fascinating feature was reported in few chaotic oscillators [35–40]. In security engineering, chaotic signals are commonly used to transmit sensitive information over an unsecured channel. Therefore, the amplitude of the chaotic signal containing this information must match the channel characteristic otherwise it will be altered. For this purpose, the amplitude of the attractors of the

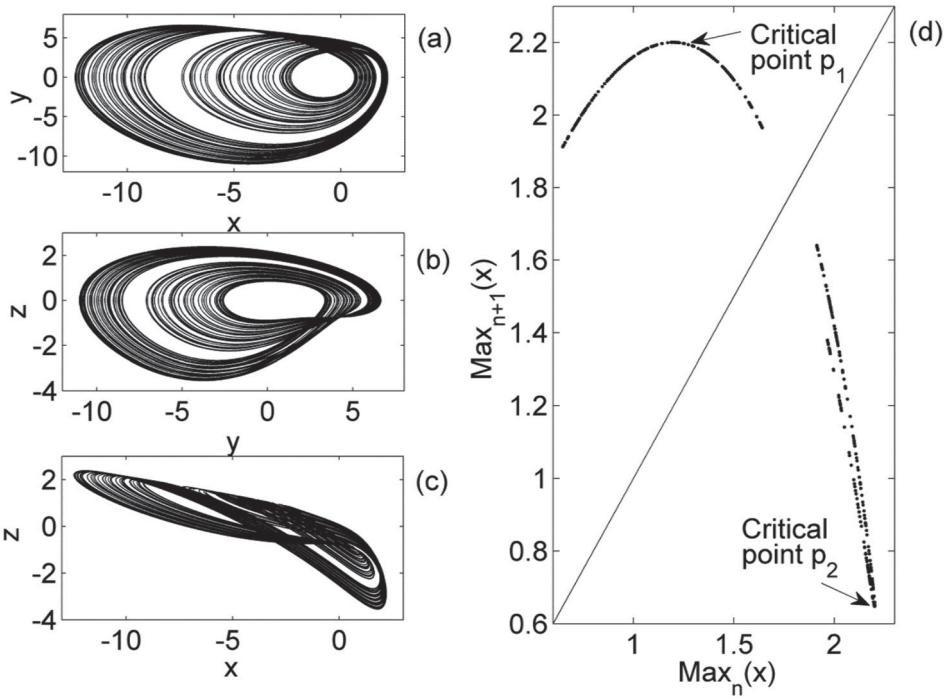

Figure 5. Phase portraits in planes (x, y) (a), (y, z) (b), (x, z) (c) and the first-return map $(\mathrm{Max}_{n+1}(x) = f\ (\mathrm{Max}_n(x)))$ of the maxima of $x(t)$ (d) for $\alpha = 0.39$ and $\beta = 5$ with initial conditions $(x(0), y(0), z(0)) = (0.1, 0.1, 0.1)$.

system (4) can be adjusted as in [35,36]. Interestingly, system (4) has feature of partial amplitude control. Indeed, the state variable x appears only in the third equation of autonomous system (4) and its amplitude can be changed by inserting a boosting controller γ into system (4) as follows:

$$\dot{x} = y, \tag{9a}$$

$$\dot{y} = \beta z, \tag{9b}$$

$$\dot{z} = -z - \alpha y + 1 - \exp(x + \gamma). \tag{9c}$$

System (9) has only one equilibrium point $E_1 = (-\gamma, 0, 0)$. The local stability of $E_1 = (-\gamma, 0, 0)$ reveals that if $\beta > 0$, system (9) has a Hopf bifurcation when α passes through the critical value $\alpha_H = 1$. So the stability of equilibrium point $E_1 = (-\gamma, 0, 0)$ is independent of boosting controller γ. In order to check the partial amplitude control of chaotic system (9), the plot of the average values of the state variables x, y and z versus boosting controller γ is shown is in Figure 6.

It is shown in Figure 6 that the average of the state variable x decreased and other two state variables (y and z) remain unchanged when boosting controller is varied. The phase portraits and time series of the state variable x of system (9) are depicted in Figure 7 for different of values of boosting controller γ.

As shown in Figure 7, the amplitude of chaotic signal x is boosted from a bipolar signal to unipolar signal when increasing boosting controller γ.

Furthermore, system (4) has also the feature of total amplitude control by inserting $x \to x/\varepsilon$, $y \to y/\varepsilon$ and $z \to z/\varepsilon$ in system (9). The parameter ε remains in

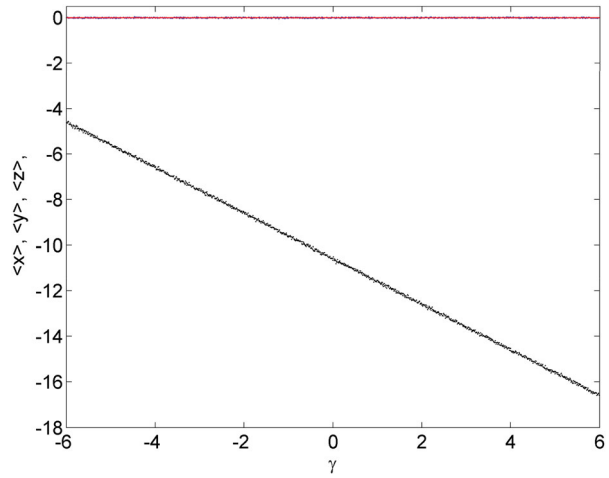

Figure 6. (Colour online) The average values of the state variables x (black), y (blue) and z (red) versus boosting controller γ for $\alpha = 0.235$ and $\beta = 5$.

the constant and exponential terms as shown in the following system (10):

$$\dot{x} = y, \tag{10a}$$

$$\dot{y} = \beta z, \tag{10b}$$

$$\dot{z} = -z - \alpha y + \varepsilon[1 - \exp(x/\varepsilon + \gamma)]. \tag{10c}$$

System (10) has only one equilibrium point $E_2 = (-\varepsilon\gamma, 0, 0)$. The local stability of $E_2 = (-\varepsilon\gamma, 0, 0)$ shows that if $\beta > 0$, system (10) has a Hopf bifurcation when α passes through the critical value $\alpha_H = 1$. So the stability of equilibrium point $E_2 = (-\varepsilon\gamma, 0, 0)$ is

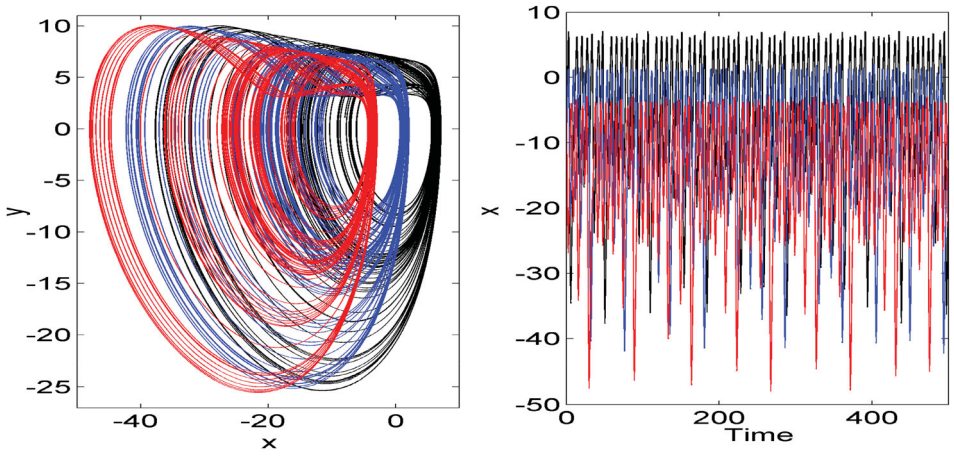

Figure 7. Phase portraits in the plane (x, y) and time series of the signal x of system (9) for $\alpha = 0.235$ and different values of control parameter γ: $\gamma = -4$ (black), $\gamma = 1$ (blue) and $\gamma = 6$ (red). Initial conditions $(x\,(0), y\,(0), z\,(0)) = (0.1, 0.1, 0.1)$.

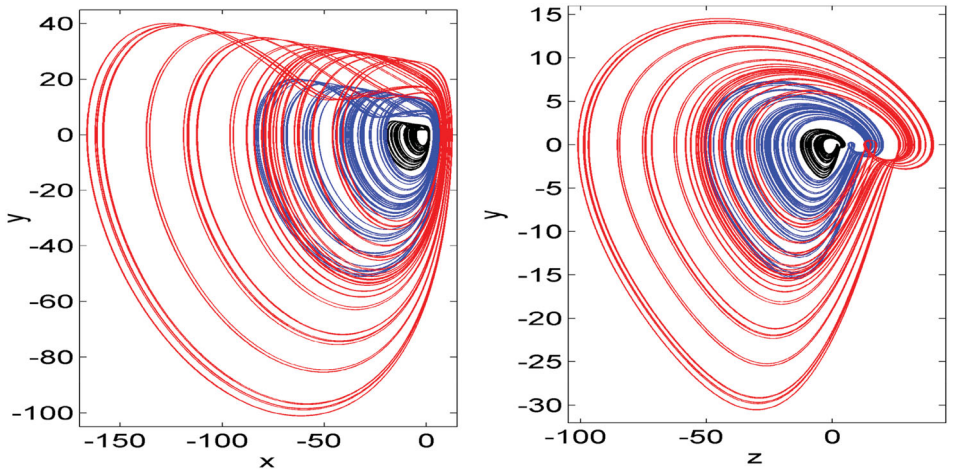

Figure 8. (Colour online) Phase portraits in the planes (x, y) and (z, y) of system (10) for $\gamma = 0, \alpha = 0.235$ and $\beta = 5$ and different values of control parameter ε: $\varepsilon = 0.5$ (black), $\varepsilon = 2$ (blue) and $\varepsilon = 4$ (red). Initial conditions $(x\,(0), y\,(0), z\,(0)) = (0.1, 0.1, 0.1)$.

independent of the parameters ε and γ. The phase portraits of system (10) are depicted in Figure 8 for different values of control parameter ε.

As shown in Figure 8, the amplitude of chaotic signals x, y and z are adjusted simultaneously by the control parameter ε. The amplitude control scheme adjusts the amplitude of the attractors for a small value (for $\epsilon = 0.5$, the amplitude is less than 10) to large values (for $\epsilon = 4$, the amplitude is greater than 30).

3. Electronic circuit realization of the autonomous Toda jerk oscillator

In this section, an electronic circuit to model the autonomous proposed Toda jerk oscillator is designed and realized (see Figure 9).

The circuit of Figure 9 is built using four operational amplifiers OP_1 to OP_4, six resistors, three capacitors C_1, C_2, C_3 of ceramic type and a simple diode D of reference 1N4148 which is used to implement the exponential nonlinearity. The expressions of voltage across the capacitors are obtained using the Kirchhoff voltage law as follows:

$$\frac{dV_x}{dt} = \frac{1}{R_1 C_1} V_y, \tag{11a}$$

$$\frac{dV_y}{dt} = \frac{1}{R_2 C_2} V_z, \tag{11b}$$

$$\frac{dV_z}{dt} = -\frac{1}{RC_3} V_z - \frac{1}{R_6 C_3} V_y - \frac{I_S}{C_3}\left(\exp\left(\frac{V_z}{\eta V_t}\right) - 1\right), \tag{11c}$$

where V_x, V_y, V_z are the output voltages of the operational amplifiers OP_1, OP_2, OP_3, respectively. The parameter $I_S = 2.862$ nA is the reversed saturation current, the parameter $\eta = 1.9$ is the scaling factor while the parameter $V_t = 26$ mVis the thermal voltage. The values of components in the circuit are selected as $C_1 = C_2 = C_3 = C = 18$ pF, $R_3 = R_4 = 10$ kΩ, $R_1 = R = 22$ MΩ, the potentiometers $R_6 = 99$ MΩ and 250 kΩ $< R_2 <$ 1.8 MΩ. Here the values of the parameters β and α can be chosen by varying the values of R_2 and R_6, respectively. The circuit of Figure 9 is studied and the phased portrait observed on the oscilloscope is shown in Figure 10.

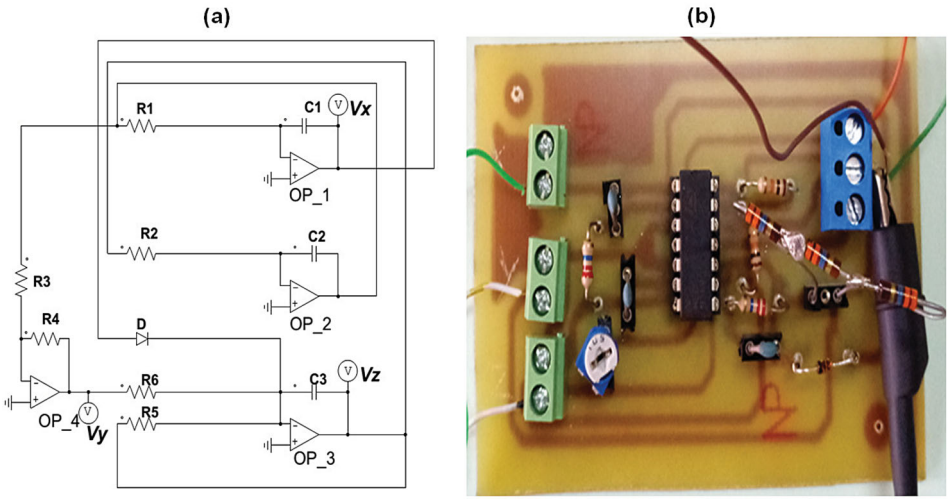

Figure 9. (Colour online) Circuit diagram (a) and experimental set-up (b) of the proposed autonomousToda jerk oscillator described by system (4): The simplicity is remarkable.

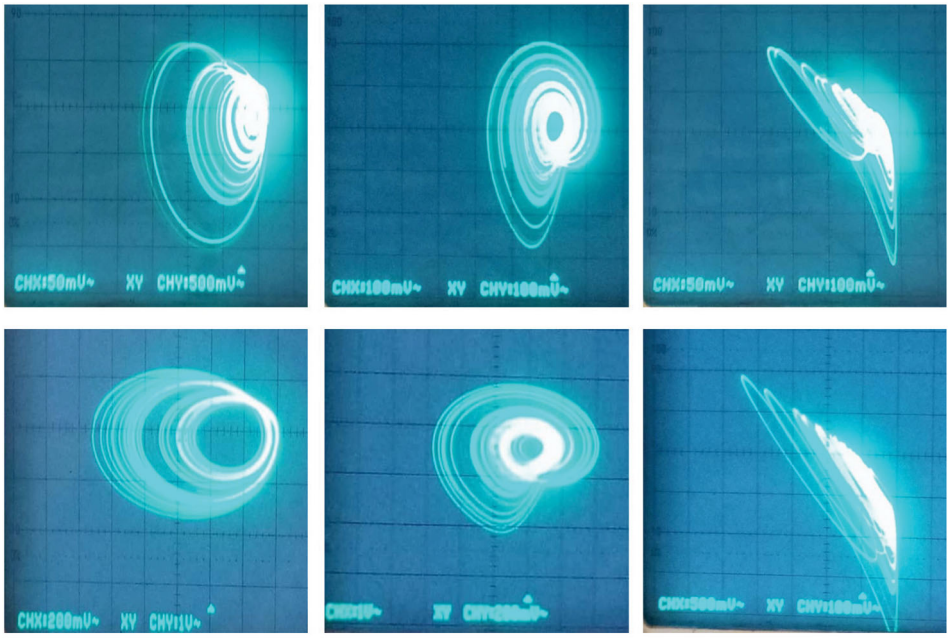

Figure 10. (Colour online) Phase portraits of the chaotic attractors obtained from the electronic circuit of Figure 9(b) and observed on the oscilloscope. In panels (1), (2) and (3), we depict the phase portraits in planes (V_x, V_y), (V_y, V_z) and (V_x, V_z), respectively. The value of resistors R_2 are $R_2 = 2.7\ \mathrm{M\Omega}$ (the first line reproduces Figure 2) and $R_2 = 866\ \mathrm{k\Omega}$ (the second line reproduces Figure 5(a)–(c)).

The reader can see in Figure 10 that the circuit of Figure 9(b) displays chaotic attractors (chaotic oscillations in the first line of Figure 10 and chaotic bubbles in the second line of Figure 10) which are similar to those obtained numerically in Figures 2 and 5(a)–(c), respectively.

4. Analysis and combination synchronization of the fractional-order autonomous chaotic Toda jerk oscillator

The fractional calculus deals with the generalization of ordinary differentiation and integration to non-integer order namely fractional-order. For many years, this branch of science was considered as a sole mathematical and theoretical subject with nearly no applications [41,42]. But, in recent decades, fractional calculus has become an interesting topic among researchers and different applications have been proposed for this field of science [43–45]. Using the notion of fractional-order in modelling and simulation of systems may be a more realistic step because real phenomena are generally fractional [46]. So, fractional-order calculus-based modelling tools enable us to describe and model real processes more accurately than the integer order methods [47,48]. For example, the capacitors are one of the crucial elements in integrated circuits and are used extensively in many electronic circuits. However, Jonscher [49] demonstrated that the ideal capacitor cannot exist in nature, because an impedance of the

form $1/(j\omega C)$ would violate causality. So, the necessity of finding more realistic models of capacitors leads to the usage of fractional calculus as a modelling tool. In this section, we consider the fractional-order of the proposed autonomous Toda jerk oscillator motivated by the fact that for realistic modelling, the electric characteristics of the capacitors used in the circuitry realization of the proposed autonomous Toda jerk oscillator (see Section 3) can include fractional-order time derivative. The mathematical description of the commensurate fractional order of the proposed autonomous Toda jerk oscillator is expressed as follows:

$$\frac{\mathrm{d}^q x}{\mathrm{d}t^q} = y, \tag{12a}$$

$$\frac{\mathrm{d}^q y}{\mathrm{d}t^q} = \beta z, \tag{12b}$$

$$\frac{\mathrm{d}^q z}{\mathrm{d}t^q} = -z - \alpha y + 1 - \exp(x), \tag{12c}$$

where q are the derivative orders satisfying $0 < q \leq 1$. There are several definitions for the fractional differential operator: first the Grünwald–Letnikov derivative is a basic extension of the natural derivative to the fractional one, which was introduced by Anton Karl Grünwald in 1867, and then by Aleksey Vasilievich Letnikov in 1868; the second, the Riemann–Liouville fractional derivative acquiring by Riemann in 1847 and the third Caputo derivative [50,51]. Riemann–Liouville fractional derivatives failed in the description and modelling of some complex phenomena. Caputo derivative was introduced in 1967 [52] and was able to describe the modelling of some complex phenomena. In the present work the authors choose the Caputo definition. The main advantage of using the Caputo definition is due to the fact that initial conditions for the fractional-order differential equations with the Caputo derivatives are in the same form as those of integer order differential equations, and there are clear interpretations of the initial conditions for integer orders [53]. In addition, it has the benefit of possessing a value of zero when it is applied to a constant.

4.1. Effect of fractional derivation on the autonomous chaotic Toda jerk oscillator

To study the effect of fractional derivation on the chaotic autonomous Toda jerk oscillator for $\alpha = 0.235$ and $\beta = 5.0$, we consider the stability condition of the equilibrium point to obtain the necessary condition of chaos occurrence. The fractional-order system (12) has a unique equilibrium point $O = (0, 0, 0)$. Evaluation of the Jacobian matrix at the equilibrium point $O = (0, 0, 0)$ yields the following eigenvalues: $\lambda_1 = -1.839228065$, $\lambda_{2,3} = 0.4196140325 \pm 1.594508035\mathrm{j}$. From [20], we can get the following inequality in order to determine the stability condition: $\arg(0.4196140325 \pm 1.594508035\mathrm{j}) > q\pi/2 \Rightarrow q < 0.8361801503$. Now according to [20], equilibrium point O is saddle point of index 2. In order to find the lowest order of system (12) to remain chaotic, we investigate numerically the dynamics of this system by plotting the bifurcation diagram illustrating the local maxima and the maximum Lyapunov exponent diagram of the state variable $x(t)$ while the fractional-order q is varied as depicted in Figure 11.

We can notice that the period-doubling cascade to chaos occurs for increasing values of q: period-1-oscillations for $q < 0.94$, period-2 for $0.94 < q < 0.98$, period-4-oscillations for $0.98 < q < 0.995$ until chaos for $0.995 < q < 1.0$. These numerical simulations reveal that for $q \geq 0.995$ the fractional-order system (12) is chaotic. Hence, it is clear that the lowest order for the commensurate fractional-order system (12) to show chaos is $3q \approx 2.985$. We present in Figure 12 the phase portraits in the planes (x, y) of significant results obtained for specific values of commensurate fractional-order q obtained from the numerical simulations of fractional-order system (12).

For $q = 0.996$, Figure 12(a) shows one-scroll chaotic attractor. Period-8-oscillations (see Figure 12(b)), period-4-oscillations (see Figure 12(c)), period-2-oscillations (see Figure 12(d)) and period-1-oscillations (see Figure 12(e)) are shown at $q = 0.994$, $q = 0.99$, $q = 0.96$ and $q = 0.9$, respectively. The fractional-order system (12) becomes non-chaotic and its trajectories converge to its equilibrium point O at $q = 0.8$ (see Figure 12(f)).

4.2. Combination synchronization of the fractional-order autonomous chaotic Toda jerk oscillator

The aim of this subsection is to provide an example of combination synchronization of three fractional-order proposed autonomous chaotic Toda jerk oscillators where the first two of them are the drive type and the third is the response oscillator. In a common drive-response scheme, the drive system is responsible for transmission of the signal, however for the combination synchronization; two chaotic systems are capable of transmitting signal which might have harder anti-hack capability than transmitted by a typical drive-response model [54–56]. The drive-response systems of fractional-order proposed autonomous Toda jerk oscillators are expressed, respectively as follows:

$$\frac{\mathrm{d}^q x_m}{\mathrm{d}t^q} = y_m, \tag{13a}$$

$$\frac{\mathrm{d}^q y_m}{\mathrm{d}t^q} = \beta z_m, \tag{13b}$$

$$\frac{\mathrm{d}^q z_m}{\mathrm{d}t^q} = -z_m - \alpha y_m + 1 - \exp(x_m), \tag{13c}$$

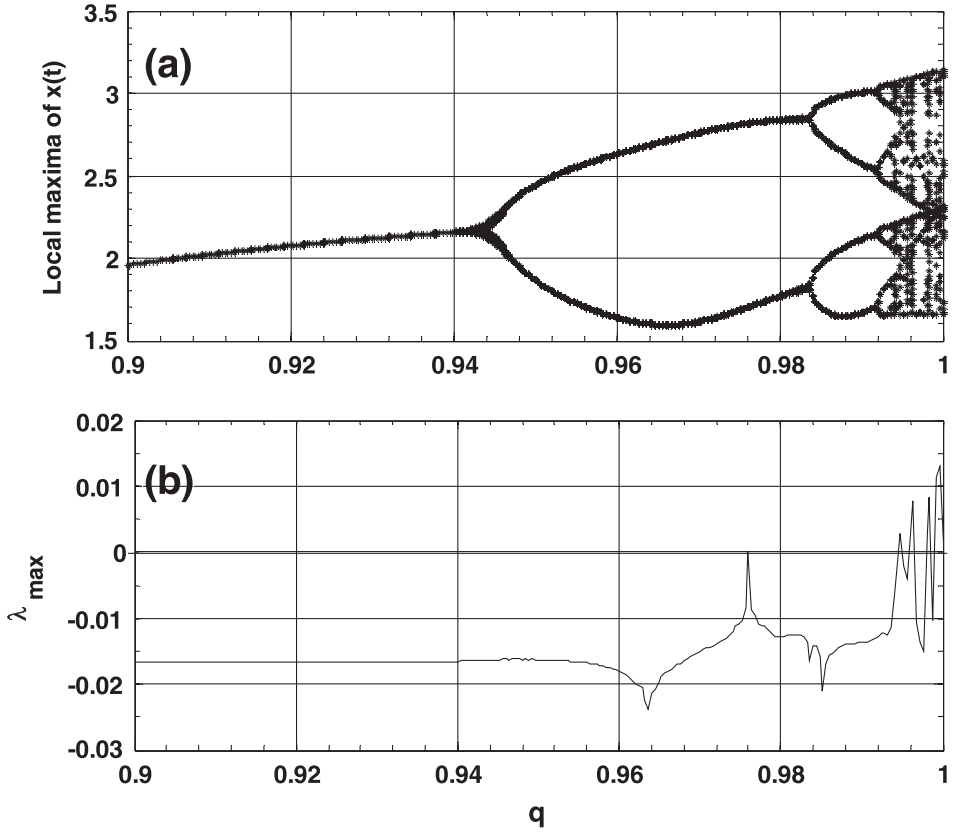

Figure 11. (a) Bifurcation diagram showing the local maxima of the state variable x and (b) the maximum Lyapunov exponent diagram versus the commensurate fractional-order q. The parameters are $\alpha = 0.235$ and $\beta = 5$. Initial conditions $(x(0), y(0), z(0)) = (0.1, 0.1, 0.1)$.

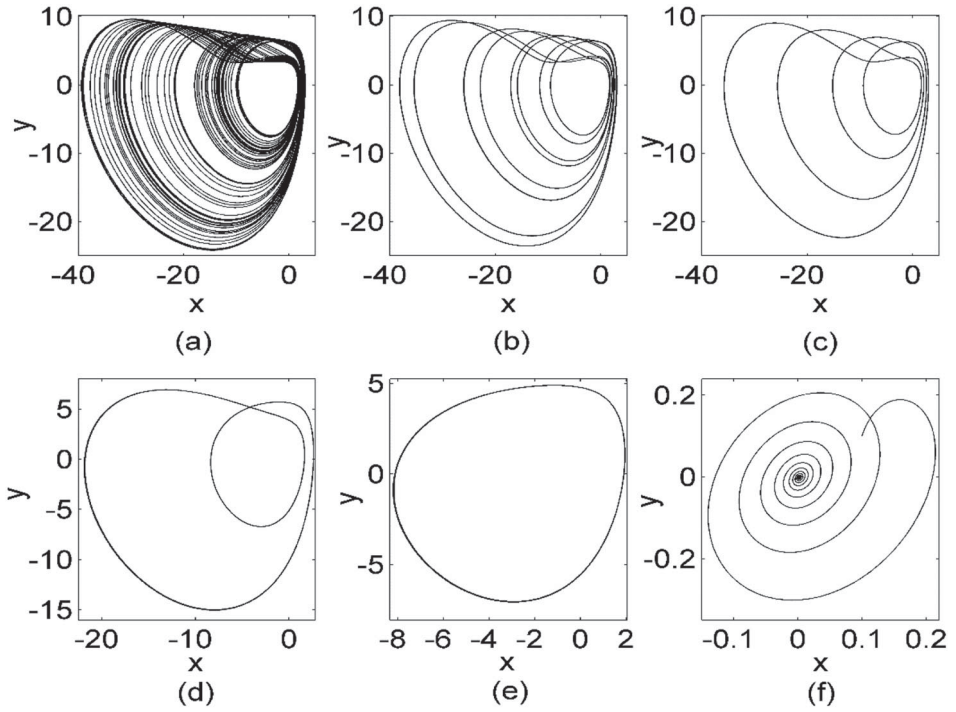

Figure 12. Phase portraits of the fractional-order system (12) with commensurate fractional-orders: (a) $q = 0.996$, (b) $q = 0.994$, (c) $q = 0.99$, (d) $q = 0.96$, (e) $q = 0.9$ and (f) $q = 0.8$. The other parameters are $\alpha = 0.235$ and $\beta = 5$. Initial conditions $(x(0), y(0), z(0)) = (0.1, 0.1, 0.1)$.

where $m = 1, 2$ and

$$\frac{\mathrm{d}^q x_s}{\mathrm{d}t^q} = y_s + u_1, \tag{14a}$$

$$\frac{\mathrm{d}^q y_s}{\mathrm{d}t^q} = \beta z_s + u_2, \tag{14b}$$

$$\frac{\mathrm{d}^q z_s}{\mathrm{d}t^q} = -z_s - \alpha y_s + 1 - \exp(x_s) + u_3, \tag{14c}$$

where u_i (i = 1,2,3) are controllers to be designed such that the three systems can be synchronized. For this purpose, let the state errors be $e = Ax + By - Cz$ where $x = (x_1, y_1, z_1)^T, y = (x_2, y_2, z_2)^T, z = (x_s, y_s, z_s)^T, e = (e_x, e_y, e_z)^T, A, B, C \in R^{3\times 3}$. Choose some suitable control functions u_i (i = 1,2,3), such that $\lim_{t\to\infty} ||Ax + By - Cz|| = 0$ then the three systems will approach synchronization. For the convenience of our discussions, we assume that A = diag(η_1,η_2,η_3), B = diag(γ_1,γ_2,γ_3), C = diag(ε_1,ε_2,ε_3), we get the error dynamical system as follows:

$$e_x = \eta_1 x_1 + \gamma_1 x_2 - \varepsilon_1 x_s, \tag{15a}$$

$$e_y = \eta_2 y_1 + \gamma_2 y_2 - \varepsilon_2 y_s, \tag{15b}$$

$$e_x = \eta_3 z_1 + \gamma_3 z_2 - \varepsilon_3 z_s. \tag{15c}$$

It is easy to see from the set of Equation (15) that the error dynamical system can be obtained as follows:

$$\frac{\mathrm{d}^q e_x}{\mathrm{d}t^q} = \eta_1 \frac{\mathrm{d}^q x_1}{\mathrm{d}t^q} + \gamma_1 \frac{\mathrm{d}^q x_2}{\mathrm{d}t^q} - \varepsilon_1 \frac{\mathrm{d}^q x_s}{\mathrm{d}t^q}, \tag{16a}$$

$$\frac{\mathrm{d}^q e_y}{\mathrm{d}t^q} = \eta_2 \frac{\mathrm{d}^q y_1}{\mathrm{d}t^q} + \gamma_2 \frac{\mathrm{d}^q y_2}{\mathrm{d}t^q} - \varepsilon_2 \frac{\mathrm{d}^q y_s}{\mathrm{d}t^q}, \tag{16b}$$

$$\frac{\mathrm{d}^q e_z}{\mathrm{d}t^q} = \eta_3 \frac{\mathrm{d}^q z_1}{\mathrm{d}t^q} + \gamma_3 \frac{\mathrm{d}^q z_2}{\mathrm{d}t^q} - \varepsilon_3 \frac{\mathrm{d}^q z_s}{\mathrm{d}t^q}. \tag{16c}$$

Substituting Equations (13), (14) and (15) into Equations (16a) to (16c) yields

$$\frac{\mathrm{d}^q e_x}{\mathrm{d}t^q} = \eta_1 y_1 + \gamma_1 y_2 - \varepsilon_1 y_s - \varepsilon_1 u_1, \tag{17a}$$

$$\frac{\mathrm{d}^q e_y}{\mathrm{d}t^q} = \beta\eta_2 z_1 + \beta\gamma_2 z_2 - \beta\varepsilon_2 z_s - \varepsilon_2 u_2, \tag{17b}$$

$$\frac{\mathrm{d}^q e_z}{\mathrm{d}t^q} = -e_x - \alpha e_y + (\eta_3 + \gamma_3 - \varepsilon_3) - [\eta_3 \exp(x_1) + \gamma_3 \exp(x_2) - \varepsilon_3 \exp(x_3)] - \varepsilon_3 u_3. \tag{17c}$$

If the controller laws are chosen as follows:

$$u_1 = (\eta_1 y_1 + \gamma_1 y_2 - \varepsilon_1 y_s - v_1)/\varepsilon_1, \tag{18a}$$

$$u_2 = (\beta\eta_2 z_1 + \beta\gamma_2 z_2 - \beta\varepsilon_2 z_s - v_2)/\varepsilon_2, \tag{18b}$$

$$u_3 = [\eta_3 + \gamma_3 - \varepsilon_3 - \eta_3 \exp(x_1) - \gamma_3 \exp(x_2) + \varepsilon_3 \exp(x_s) - v_3]/\varepsilon_3, \tag{18c}$$

where v_i are chosen by suitable linear functions of the errors terms $e_i (i = x, y, z)$, we choose it such that the error dynamics become stable. The general form of such functions is as follows:

$$\begin{pmatrix} v_x \\ v_y \\ v_z \end{pmatrix} = \bar{A} \begin{pmatrix} e_x \\ e_y \\ e_z \end{pmatrix}, \tag{19}$$

where $A = \begin{pmatrix} a_{11} & a_{12} & a_{13} \\ a_{21} & a_{22} & a_{23} \\ a_{31} & a_{32} & a_{33} \end{pmatrix}$ is a 3×3 real matrix. Based on the v_i, we need to make the conditions $|\arg(\lambda_i)| > q\pi/2$ satisfied where λ_i are eigenvalues of the error dynamical system. If we choose $a_{11} = 0$, $a_{12} = 1$, $a_{13} = 0$, $a_{21} = 0$, $a_{22} = 0$, $a_{23} = 8.5$, $a_{31} = -1$, $a_{32} = -1.765$, $a_{33} = -2$, then the error

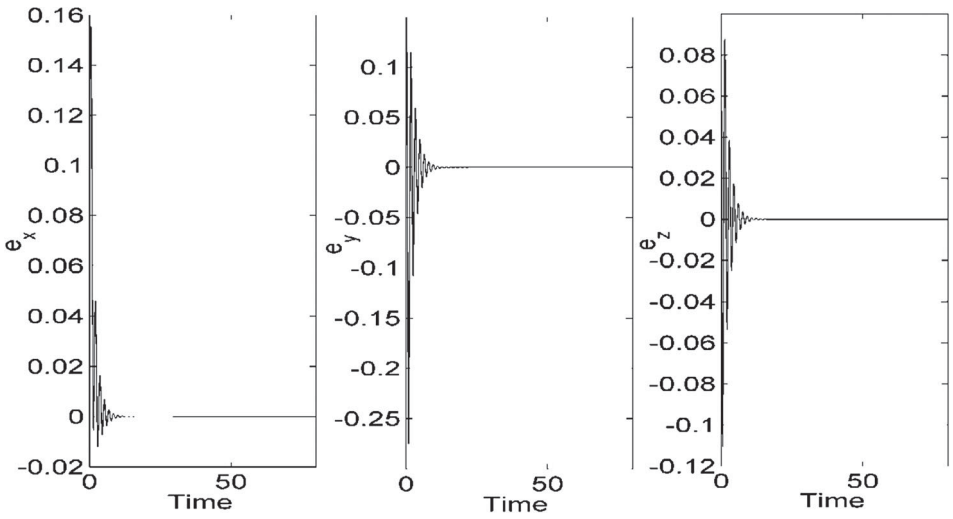

Figure 13. Synchronization errors between the drive and response Toda jerk oscillators (13) and (14) for $\alpha = 0.235$, $\beta = 5$, $q = 0.996$ and the control parameters $\eta_1 = \eta_2 = \eta_3 = 1, \gamma_1 = \gamma_2 = \gamma_3 = 1, \varepsilon_1 = \varepsilon_2 = \varepsilon_3 = 0.5$.

dynamical system is

$$\frac{\mathrm{d}^q e_x}{\mathrm{d}t^q} = e_y, \tag{20a}$$

$$\frac{\mathrm{d}^q e_y}{\mathrm{d}t^q} = 8.5e_z, \tag{20b}$$

$$\frac{\mathrm{d}^q e_z}{\mathrm{d}t^q} = -2e_x - (1.765 + \alpha)e_y - 2e_z. \tag{20c}$$

Since $\alpha = 0.235$ and $q = 0.996$, we get three eigenvalues $\lambda_1 = -1.06224279, \lambda_2 = -0.4688786033 + 3.972911655\mathrm{j}$ and $\lambda_3 = -0.4688786033 - 3.972911655\mathrm{j}$ which satisfy $|\arg(\lambda_i)| = 1.688271805 > 0.498\pi$. This ensures that the error states asymptotically converge to zero as $t \to \infty$ and therefore the combination synchronization between the drive-response systems (13) and (14) is achieved. For the purpose of numerical simulations, we set $\alpha = 0.235, \beta = 5$ and $q = 0.996$ with the initial conditions of the drive and response Toda jerk oscillators: $(x_1(0), y_1(0), z_1(0)) = (0.1, 0.1, 0.1)$, $(x_2(0), y_2(0), z_2(0)) = (-0.1, -0.1, -0.1)$ and $(x_s(0), y_s(0), z_s(0)) = (-0.2, -0.2, -0.2)$ to ensure chaotic oscillations. In Figure 12, the synchronization errors between the drive and response proposed autonomous Toda jerk oscillators (13) and (14) are plotted in order to check the effectiveness of the design controllers.

Form Figure 13, one can see the asymptotical convergence of the error states to zero. As shown in the numerical simulations, the design controllers can synchronize the drive and response proposed autonomous Toda jerk oscillators (13) and (14).

5. Conclusion

This article reported results on the analysis of an autonomous Toda jerk oscillator and combination synchronization of its fractional-order form. By using the Routh–Hurwitz stability criterion and linear stability of the only equilibrium point, it was found that Hopf bifurcation occurs in the proposed autonomous Toda jerk oscillator. For specific parameters, the proposed autonomous Toda jerk oscillator exhibited one-scroll chaotic attractor, antimonotonicity, periodic and chaotic bubbles. By adding two new parameters in the proposed autonomous Toda jerk oscillator, a flexible chaotic autonomous jerk oscillator with partial or total amplitude control was achieved. One-scroll and bubble chaotic attractors obtained during numerical simulations were confirmed using electronic circuit realization of the proposed autonomous Toda jerk oscillator. Chaos was shown to exist in the fractional-order Toda jerk oscillator with orders less than three. Using the nonlinear feedback control technique, combination synchronization was obtained between drive-response fractional-order of the proposed autonomous chaotic Toda jerk oscillators. Conditions for achieving chaos synchronization of fractional-order of the proposed autonomous chaotic Toda jerk oscillators were illustrated and numerical simulations were carried out to verify the analytical study. This work reveals that the proposed autonomous Toda jerk oscillator can generate self-excited attractors when its parameter $\alpha < 1$ because its only equilibrium point is unstable for $\alpha < 1$. Since its only equilibrium point is stable for $\alpha > 1$, the investigation of hidden attractors in the proposed autonomous Toda jerk oscillator should be further done in future works.

Acknowledgements

The authors wish to thank Dr V. Kamdoum Tamba (University of Dschang, Cameroon) for having kindly providing the literature on antimonotonicity phenomenon.

Disclosure statement

No potential conflict of interest was reported by the authors.

References

[1] Ahmad I, Shafiq M, Al-Sawalha M. Globally exponential multiswitching-combination synchronization control of chaotic systems for secure communications. Chin J Phys. 2018. doi:10.1016/j.cjph.2018.03.011
[2] Otto E. Chaos in dynamical systems. Cambridge: Cambridge University Press; 1993.
[3] Hilborn RC. Chaos and nonlinear dynamics: an introduction for scientists and engineers. New york: Oxford University Press; 2006.
[4] Xiaofan W, Guanrong C. Chaotification via arbitrarily small feedback controls: theory, method, and applications. Int J Bifurcat Chaos. 2000;10:549–570.
[5] Liu H, Wang X, Zhu Q. Asynchronous anti-noise hyper chaotic secure communication system based on dynamic delay and state variables switching. Phys Lett A. 2011;375:2828–2835.
[6] Sprott JC. A new class of chaotic circuit. Phys Lett A. 2000;266:19–23.
[7] Sprott JC. Simple chaotic systems and circuits. Am J Phys. 2000;68:758–763.
[8] Sprott JC. Elegant chaos: algebraically simple flow. Singapore: World Scientific Publishing; 2010.
[9] Acho L, Rolon J, Benitez S. A chaotic oscillator using the Van der Pol dynamic immersed into a Jerk system. WSEAS Trans Circuits Syst. 2004;3:198–209.
[10] Benítez MS, Zuppa LA, Guerra RJR. Chaotification of the Van der Pol system using jerk architecture. IEICE Trans Fundam. 2006;E89:A375–A378.
[11] Louodop P, Kountchou M, Fotsin H, et al. Practical finite-time synchronization of jerk systems: theory and experiment. Nonlinear Dyn. 2014;78:597–607.
[12] Kengne J, Njitacke ZT, Fotins HB. Dynamical analysis of a simple 3-D autonomous jerk system with multiple attractors. Nonlinear Dyn. 2016;83:751–765.
[13] Kengne J, Njitacke ZT, Nguomkam Negou A, et al. Coexistence of multiple attractors and crisis route to chaos in a novel chaotic jerk circuit. Int J Bifurc Chaos. 2015;26:1650081–1650098.
[14] Goswami BK. Observation of some new phenomena involving period tripling and period doubling. Int J Bifurcat Chaos. 1995;5:303–312.

[15] Goswami BK, Pisarchik AN. Controlling multistability by small periodic perturbation. Int J Bifurcat Chaos. 2008;18:1645–1673.
[16] Cialdi S, Castelli F, Prati F. Lasers as Toda oscillators: An experimental confirmation. Opt Commun. 2013;287:176–179.
[17] Klinker T, Meyer-Ilse W, Lauterborn W. Period doubling and chaotic behavior in a driven Toda oscillator. Phys Lett A. 1984;101A:371–375.
[18] Nana B, Woafo P, Domngang S. Chaotic synchronization with experimental application to secure communications. Commun Nonlinear Sci Numer Simul. 2009;14:2266–2276.
[19] Kingni ST, Talla Mbé JH, Woafo P. Semiconductor lasers driven by self-sustained chaotic electronic oscillators and applications to optical chaos cryptography. Chaos. 2012;22:033108–033115.
[20] Tavazoei MS, Haeri M. A necessary condition for double scroll attractor existence in fractional-order systems. Phys Lett A. 2007;367:102–113.
[21] Hilfer R. Applications of fractional calculus in physics. New Jersey: World Scientific; 2001.
[22] Caponetto R, Dongola R, Fortuna L, et al. Fractional-order system: modelling and control applications. World Sci Ser Nonlinear Science, Series A. 2010;200.
[23] Diethelm K, Ford NJ, Freed D. A predictor–corrector approach for the numerical solution of fractional differential equations. Nonlinear Dyn. 2002;29:3–22.
[24] Gottlieb HPW. Question #38. What is the simplest jerk function that gives chaos? Am J Phys. 1996;64:525.
[25] Sprott JC. A new chaotic jerk circuit. IEEE Trans Circuits Syst II Express Briefs. 2011;58:240–243.
[26] Malasoma JM. What is the simplest dissipative chaotic jerk equation which is parity invariant? Phys Lett A. 2000;264:383–389.
[27] Sprott JC. Some simple chaotic jerk functions. Am J Phys. 1997;65:537–543.
[28] Campos-Canton E, Barajas-Ramırez JG, Solıs-Perales G, et al. Multiscroll attractors by switching systems. Chaos. 2010;20:013116.
[29] Campos-Canton E, Femat R, Chen G. Attractors generated from switching unstable dissipative systems. Chaos. 2012;22:033121.
[30] Aguirre-Hernandez B, Campos-Canton E, Lopez-Renterıa JA, et al. A polynomial approach for generating a monoparametric family of chaotic attractors via switched linear systems. Chaos Solitons Fractals. 2015;71:100–106.
[31] Bier M, Boutis TC. Remerging Feigenbaum trees in dynamica systems. Phys Lett A. 1984;104:239–244.
[32] Kyprianidis IM, Stouboulos IN, Haralabidis P. Antimonotonicity and chaotic dynamics in a fourth-order autonomous nonlinear electric circuit. Int J Bifurc Chaos. 2000;10:1903–1911.
[33] Dawson SP, Grebogi C, Kan I, et al. Antimonotonicity: inevitable reversals of period-doubling cascades. Phys Lett A. 1992;162:249–254.
[34] Dawson SP, Grebogi C, Kocak H. Geometric mechanism for antimonotonicity in scalar maps with two critical points. Phys Rev E. 1993;48:1676–1680.
[35] Li C, Sprott JC. Amplitude control approach for chaotic signals. Nonlinear Dyn. 2013;73:1335–1341.
[36] Li C, Sprott JC. Variable-boostable chaotic flows. Optik Int J Light Electron Opt. 2016;27:10389–10398.
[37] Akif A, Chunbiao L, Ihsan P. Amplitude control analysis of a four-wing attractor, its electronic circuit designs and microcontroller-based random number generator. J Circuits Syst Comput. 2017;26:1750190–1750209.
[38] Li C, Sprott J, Yuan Z, et al. Constructing chaotic systems with total amplitude control. Int J Bifurcation Chaos. 2015;25:1530025–1530039.
[39] Li C, Wang J, Hu W. Absolute term introduced to rebuild the chaotic attractor with constant Lyapunov exponent spectrum. Nonlinear Dyn. 2012;68:575–587.
[40] Kamdoum Tamba V, Karthikeyan R, Pham V-T, et al. Chaos in a system with an absolute nonlinearity and chaos synchronization. Adv Math Phys. 2018. doi:10.1155/2018/5985489
[41] Petráš I. Fractional-order nonlinear systems: modeling, analysis and simulation. Berlin: HEP, Springer; 2011. (Nonlinear physical science).
[42] Steinhaus B. Estimating cardiac transmembrane activation and recovery times from unipolar and bipolar extracellular electrograms: a simulation study. Circ Res. 1989;64:449–462.
[43] Schafer I, Kruger K. Modelling of lossy coils using fractional derivatives. J Phys D: Appl Phys. 2008;41:1–8.
[44] Faraji S, Tavazoei MS. The effect of fractionality nature in differences between computer simulation and experimental results of a chaotic circuit. Cent Eur J Phys. 2013;11:836–844.
[45] Preda L, Mihailescu M, Preda A. Application of fractional derivative to the relaxation of laser target. UPB Sci Bull Ser A. Appl Math Phys. 2009;71:11–20.
[46] Cun-Fang F, Yan-Rong T, Ying-Hai W, et al. Active backstepping control of combined projective synchronization among different nonlinear systems. Automatika. 2017;58(3):295–301. doi:10.1080/00051144.2018.1432466.
[47] Kengne R, Tchitnga R, Tchagna Kouanou A, et al. Dynamical properties and finite-time hybrid projective synchronization using fractional nonsingular sliding mode surface in fractional-order two-stage Colpitts oscillators. J Chaos (Hindawi). 2013;839038:12.
[48] Kengne R, Tchitnga R, Mabekou S, et al. On the relay coupling of three fractional-order oscillators with time-delay consideration: Global and cluster synchronizations. Chaos Solitons Fractals. 2018;111:6–17.
[49] Jonscher AK. Dielectric relaxation in solids. London: Chelsea Dielectric Press; 1993.
[50] Podlubny I. Fractional differential equations. San Diego: Academic Press; 1999.
[51] Herrmann R. Fractional calculus: an introduction for physicists. Singapore: World Scientific; 2011. (1993).
[52] Caputo M. Linear models of dissipation whose Q is almost frequency independent—II. Geophys J Int. 1967;13:529–539.
[53] Podlubny I, El- Sayed AMA. On two definitions of fractional calculus, Pre-print UEF 03-96, ISBN 80-7099-252-2, Institute of Experimental Physics, Slovak Academy of Science, 1996.
[54] Luo RZ, Wang YL, Deng SC. Combination synchronization of three classic chaotic systems using active back stepping design. Chaos. 2011;21:043114–043120.
[55] Luo RZ, Wang YL. Finite-time stochastic combination synchronization of three different chaotic systems and its application in secure communication. Chaos. 2012;22:023109–023119.
[56] Alam Z, Yuan L, Yang Q. Chaos and combination synchronization of a new fractional-order system with two stable node-foci. IEEE/CAA J Autom Sin. 2016;3:157–164.